Applied Surface Science 305 (2014) 753–759

Contents lists available at ScienceDirect

Applied Surface Science

journal homepage: www.elsevier.com/locate/apsusc

Preparation and photocatalytic activity of $Mg_xZn_{1-x}O$ thin films on silicon substrate through sol–gel process

Changlong Liu[a,b], Fengjiao Shang[b], Guangcai Pan[b], Feng Wang[b], Zhitao Zhou[b], Wanbing Gong[b,d], Zhenfa Zi[b], Yiyong Wei[b], Xiaoshuang Chen[a,*], Jianguo Lv[a,b,c,**], Gang He[c], Miao Zhang[c], Xueping Song[c], Zhaoqi Sun[c,***]

[a] National Laboratory for Infrared Physics, Shanghai Institute of Technical Physics, Chinese Academy of Sciences, Shanghai 200083, China
[b] School of Electronic and Information Engineering, Hefei Normal University, Hefei 230061, China
[c] School of Physics and Material Science, Anhui University, Hefei 230039, China
[d] Institute of Solid State Physics, Chinese Academy of Sciences, Hefei 230031, China

ARTICLE INFO

Article history:
Received 7 January 2014
Received in revised form 2 March 2014
Accepted 30 March 2014
Available online 12 April 2014

Keywords:
$Mg_xZn_{1-x}O$ thin films
Fourier transform infrared spectrum
Photoluminescence spectrum
Photocatalytic activity

ABSTRACT

Magnesium doped zinc oxide ($Mg_xZn_{1-x}O$) thin films were synthesized on silicon substrate through sol–gel process. $Mg_{0.15}Zn_{0.85}O$ thin films were annealed at 500–800 °C and ZnO, $Mg_{0.1}Zn_{0.9}O$, $Mg_{0.05}Zn_{0.95}O$ thin films were annealed at 600 °C for 60 min, respectively. The results show that all the samples are of a hexagonal wurtzite structure of ZnO. The surface morphology is strongly dependent on mean grain size and surface fluctuation. Fourier transform infrared spectra reveal that the vibration peak at 420 cm^{-1} is of the intrinsic lattice absorption of ZnO. The peak at 1083 cm^{-1} belongs to Si—O—Si asymmetric stretching vibration. Photoluminescence spectra show that the ultraviolet emission (365–400 nm) and the broad visible emission (469–569 nm) are observed. In particular, $Mg_{0.05}Zn_{0.95}O$ thin film annealed at 600 °C exhibits the highest photocatalytic activity, degrading MO by almost 85.8% after 180 min illumination. The photocatalytic activity of the thin film is a synergistic effect defined by grain size, roughness factor, oxygen defects and amorphous MgO.

1. Introduction

Zinc oxide (ZnO) is a kind of II–VI direct wide band gap semiconductor material. Owing to its wide band gap (3.37 eV at room temperature) and large exciton binding energy (60 meV) that allows an efficient excitonic emission even at room temperature, ZnO has many potential applications in transparent electrodes [1,2], gas sensors [3,4], surface acoustic wave devices [5], the electric induced fluorescence devices and ultraviolet detectors. Many different methods have been employed to fabricate high quality ZnO thin films such as chemical vapor deposition (CVD), pulsed laser deposition (PLD), molecular beam epitaxy (MBE) [6] and sol–gel technique [7]. The sol–gel method is a simple and easy dip-coating means to obtain large area high quality ZnO thin films without complicated instruments.

The effective ionic radius of 0.57 Å for Mg^{2+} is close to that of 0.61 Å for Zn^{2+}. As a result, the incorporation of Mg^{2+} in ZnO is not expected to induce obvious change of lattice sizes [8], and most importantly, Mg doping can highly vary a continuous tailoring of optical band gap of ZnO [9,10]. It is well known that ZnO can be as efficient as TiO_2 in the photocatalytic degradation of some dyes in aqueous solution [11,12]. Therefore, ZnO thin film has been paid much attention in the degradation and complete mineralization of environment pollutant [13]. Some works have reported the photocatalytic activity of ZnO powders, nanoparticle and colloids [14–16]. But for their removal from water is difficult, ZnO thin films can be beneficial to avoid the separation of the catalyst.

In this paper, $Mg_xZn_{1-x}O$ with different concentration ($x = 0$, 0.05, 0.1, 0.15) were synthesized by a sol–gel method. The influence of Mg doping and annealing temperature on microstructure and surface morphology of the thin films were investigated. The infrared spectroscopy and photoluminescence of the thin films were studied. The photocatalytic activities of the thin films were tested and its possible mechanisms were also discussed.

* Corresponding author. Tel.: +86 21 25051403; fax: +86 21 25051403.
** Corresponding author at: School of Electronic and Information Engineering, Hefei Normal University, Hefei 230061, China. Tel.: +86 551 63674132; fax: +86 551 63674131.
*** Corresponding author. Tel.: +86 551 65107284; fax: +86 551 65107237.
E-mail addresses: xschen@mail.sitp.ac.cn (X. Chen), lvjg1@163.com (J. Lv), szq@ahu.edu.cn (Z. Sun).

http://dx.doi.org/10.1016/j.apsusc.2014.03.192
0169-4332/

2. Experimental

2.1. Sample preparation

All reagents are of analytical grade and used as received without any further purification. In our experiment, zinc acetate dehydrate [$Zn(CH_3COO)_2{\cdot}2H_2O$] and magnesium acetate tetrahydrate [$Mg(CH_3COO)_2{\cdot}4H_2O$] were dissolved into 80 ml ethylene glycol monomethyl ether at room temperature. Monoethanol amine (MEA) was used as the stabilizing agent. The molar ratio of MEA to zinc acetate dehydrate was kept as 1:1. The molar ratio of magnesium acetate to zinc acetate was 0.00, 0.05, 0.10, and 0.15, respectively. They were mixed rapidly, and stirred at 60 °C for 120 min to get a clear, homogeneous and transparent sol. The silicon substrates (15 mm × 15 mm) were cleaned ultrasonically in acetone and deionized water, and dried in hot air. Spin coating was usually made one day after the solution was prepared. $Mg_xZn_{1-x}O$ thin films were deposited on Si substrate by spin coating with 3000 rpm for 30 s. After coating, the substrates were dried at 150 °C for 10 min to remove the solvent. This procedure was repeated ten times to get the required thickness. Then the as-deposited thin films were inserted to a furnace and annealed in ambient atmosphere.

The microstructure of the thin films was analyzed by a MACM18XHF X-ray diffractometer (XRD) with Cu Kα radiation source (λ = 0.15405 nm). The surface morphology was characterized by a CSPM4000 atomic force microscopy (AFM) by using contacting mode taken over a scale of 3 μm × 3 μm. The photoluminescence (PL) spectra were investigated with a F-4500 fluorescence (FL) spectrometer at room temperature (RT). The wavelength of excitation light was 325 nm. The Fourier transform infrared (FTIR) spectra of the samples were recorded using a BRUKER VERTEX 80 Fourier transform infrared spectrophotometer over the range 4000–400 cm^{-1}.

2.2. Photocatalytic activity

Methyl orange ($CH_{14}N_{14}Na_3O_3S$), a widespread used dye, was employed as a typical dye pollutant to evaluate the photocatalytic activity of $Mg_xZn_{1-x}O$ thin films. The experiment was operated in a 25 ml glass container. The $Mg_xZn_{1-x}O$ thin films, prepared on Si substrate, were immersed in 5 ml 5 ppm methyl orange solutions and were irradiated with a 36 W low pressure mercury lamp. The distance between the low pressure mercury lamp and the sample was 10.0 cm. The absorbance of the methyl orange solution was measured at intervals of 30 min and the total illumination time was 180 min. The absorbance of methyl orange at 464 nm was directly proportional to concentration in the previous study [17]. Therefore, the absorbance of the peak at 464 nm is used to evaluate the absorption of methyl orange solution with different concentration.

The degree of photocatalytic degradation could be evaluated by measuring the absorbance of the solutions at 464 nm. The degradation efficiency of methyl orange was calculated using the equation [17]:

$$\text{Degradation efficiency}(\%) = \frac{C_0 - C_t}{C_0} \times 100 = \frac{A_0 - A_t}{A_0} \times 100 \qquad (1)$$

where C_0 and C_t are the initial and residual dye concentration after t min reaction, A_0 and A_t represents the initial absorbance and residual dye absorbance after t min reaction of the methyl orange at the characteristic absorption wavelength of 464 nm.

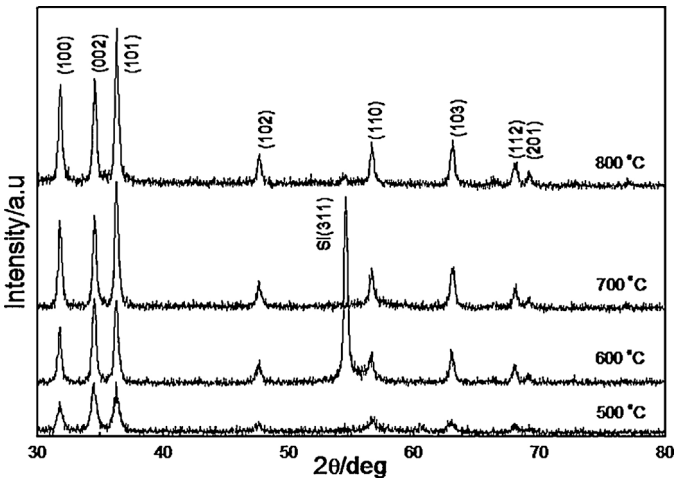

Fig. 1. XRD patterns of $Mg_{0.15}Zn_{0.85}O$ thin film at different annealing temperature.

3. Results and discussion

3.1. Microstructure and surface morphology of $Mg_xZn_{1-x}O$ thin films

Fig. 1 shows XRD patterns of the $Mg_{0.15}Zn_{0.85}O$ thin films at different annealing temperature. Fig. 2 shows XRD patterns of $Mg_xZn_{1-x}O$ thin films (x = 0, 0.05, 0.10, 0.15) annealed at 600 °C. It can be seen that all the diffraction peaks can be indexed to the hexagonal phase ZnO (JCPDS36-1451) except for the (3 1 1) diffraction peak of cubic phase Si, and no Mg or MgO peaks were detected. The results indicate that the $Mg_xZn_{1-x}O$ thin films possess a polycrystalline hexagonal wurtzite crystal structure. Mg^{2+} ions were successfully incorporated into the ZnO host lattice and substituted for Zn^{2+} ions. The mean grain size (D) can be calculated by the following Scherrer formula [18]:

$$D = \frac{0.9\lambda}{\beta \cos\theta} \qquad (2)$$

where λ, θ and β are X-ray wavelength (λ = 0.15405 nm), Bragg diffraction angle and the full width at half maximum (FWHW) of peak, respectively. The D values of the thin films were listed in Table 1. It can be seen that mean grain size of $Mg_{0.15}Zn_{0.85}O$ thin films increases from 22.3 to 28.8 nm firstly and then decreases to 27.3 nm as the annealing temperature increases from 500 to 800 °C.

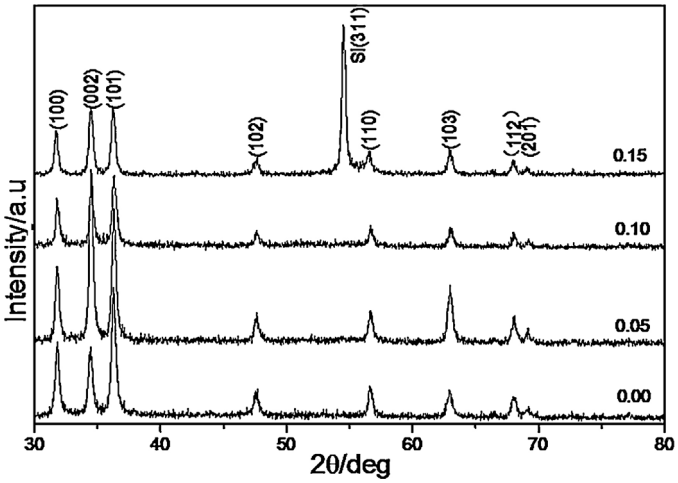

Fig. 2. XRD patterns of $Mg_xZn_{1-x}O$ thin film annealed at 600 °C: x = 0.00, 0.05, 0.10, 0.15.

Table 1
Parameter of $Mg_xZn_{1-x}O$ thin films at different annealing temperature.

Sample	Annealing temperature (°C)	*D* (nm)	RMS roughness (nm)	*r*	Degradation efficiency
$Mg_{0.15}Zn_{0.85}O$	500	22.3	6.0	1.0155	76.0
$Mg_{0.15}Zn_{0.85}O$	600	25.1	8.3	1.0197	80.2
$Mg_{0.15}Zn_{0.85}O$	700	28.8	9.1	1.0159	75.8
$Mg_{0.15}Zn_{0.85}O$	800	27.3	10.4	1.0222	71.9
$Mg_{0.1}Zn_{0.9}O$	600	27.8	9.8	1.0223	81.6
$Mg_{0.05}Zn_{0.95}O$	600	27.7	7.2	1.0210	85.8
ZnO	600	24.8	11.0	1.0161	60.4

The mean grain size of the $Mg_xZn_{1-x}O$ thin films annealed at 600 °C increases from 24.8 to 27.8 nm and then decreases to 25.1 as Mg doping increases from 0 to 0.15. The results show that lower Mg doping and annealing temperature can promote grain growth and improve the crystallite quality of the $Mg_xZn_{1-x}O$ thin films. But higher Mg doping and annealing temperature may inhibit grain growth and reduce the crystallite quality of the thin films.

Fig. 3 shows AFM images of $Mg_{0.15}Zn_{0.85}O$ thin film at different annealing temperature. The root mean squares (RMS) roughness values of $Mg_{0.15}Zn_{0.85}O$ thin film annealed at 500, 600, 700, 800 °C are 6.0, 8.3, 9.1, 10.4 nm, respectively. It can be seen that the RMS roughness of the thin film increases with the increase of annealing temperature. The change of RMS roughness of the thin films can be attributed to the change of mean grain size [19]. Fig. 4 shows AFM images of $Mg_xZn_{1-x}O$ thin film annealed at 600 °C. The root mean squares (RMS) roughness values of ZnO, $Mg_{0.05}Zn_{0.95}O$, $Mg_{0.1}Zn_{0.9}O$, $Mg_{0.15}Zn_{0.85}O$ thin film annealed at 600 °C are 11.0, 7.2, 9.8, 8.3 nm, respectively. The mean grain size and surface fluctuation of the thin films increase as Mg doping. Change of the RMS roughness can be attributed to the synergistic effect of mean grain size and surface fluctuation [20]. Roughness factor *r* [21], which is defined as the ratio of the actual area of a rough surface to the

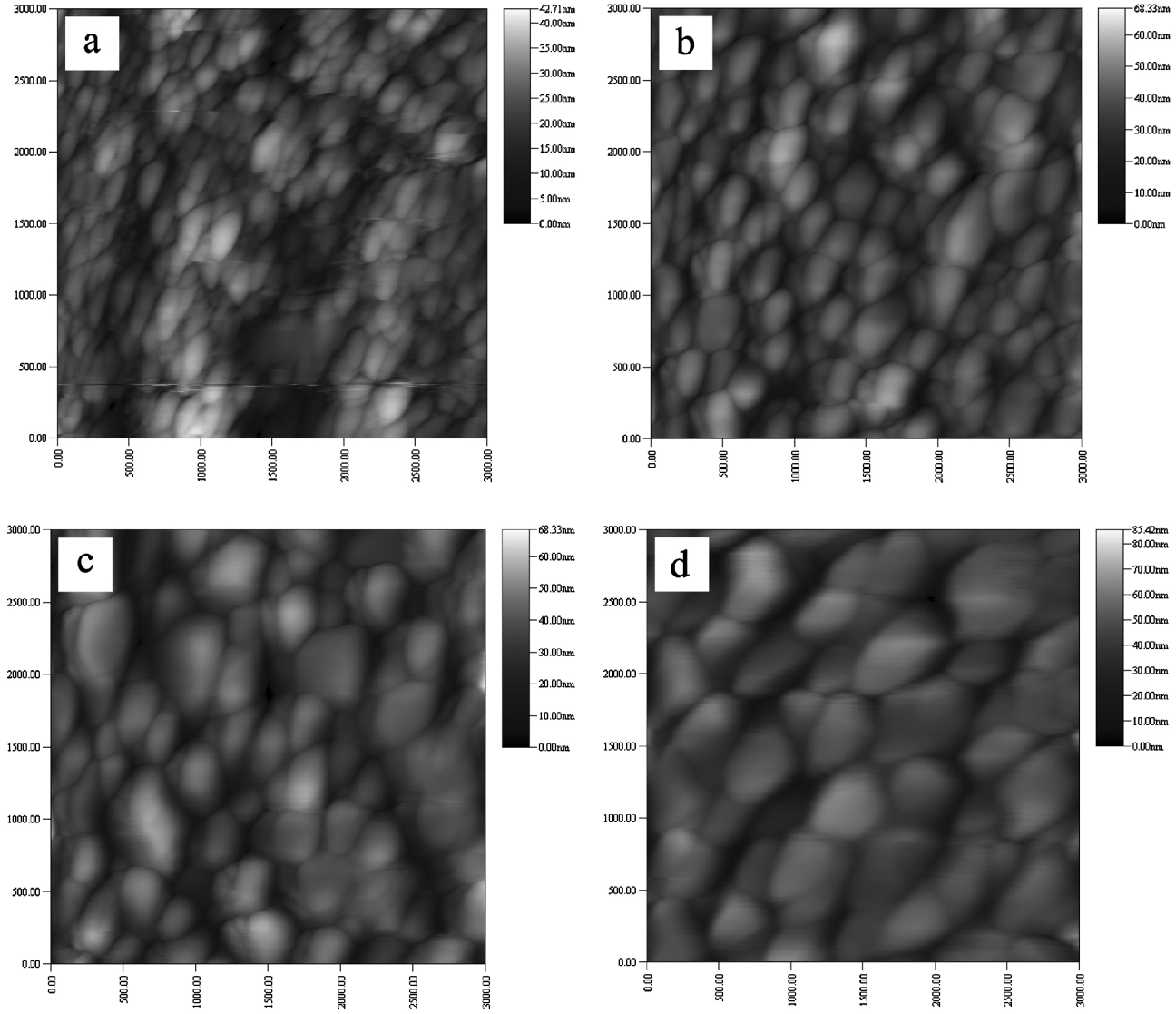

Fig. 3. AFM images of $Mg_{0.15}Zn_{0.85}O$ thin film at different annealing temperature: (a) 500 °C, (b) 600 °C, (c) 700 °C, (d) 800 °C.

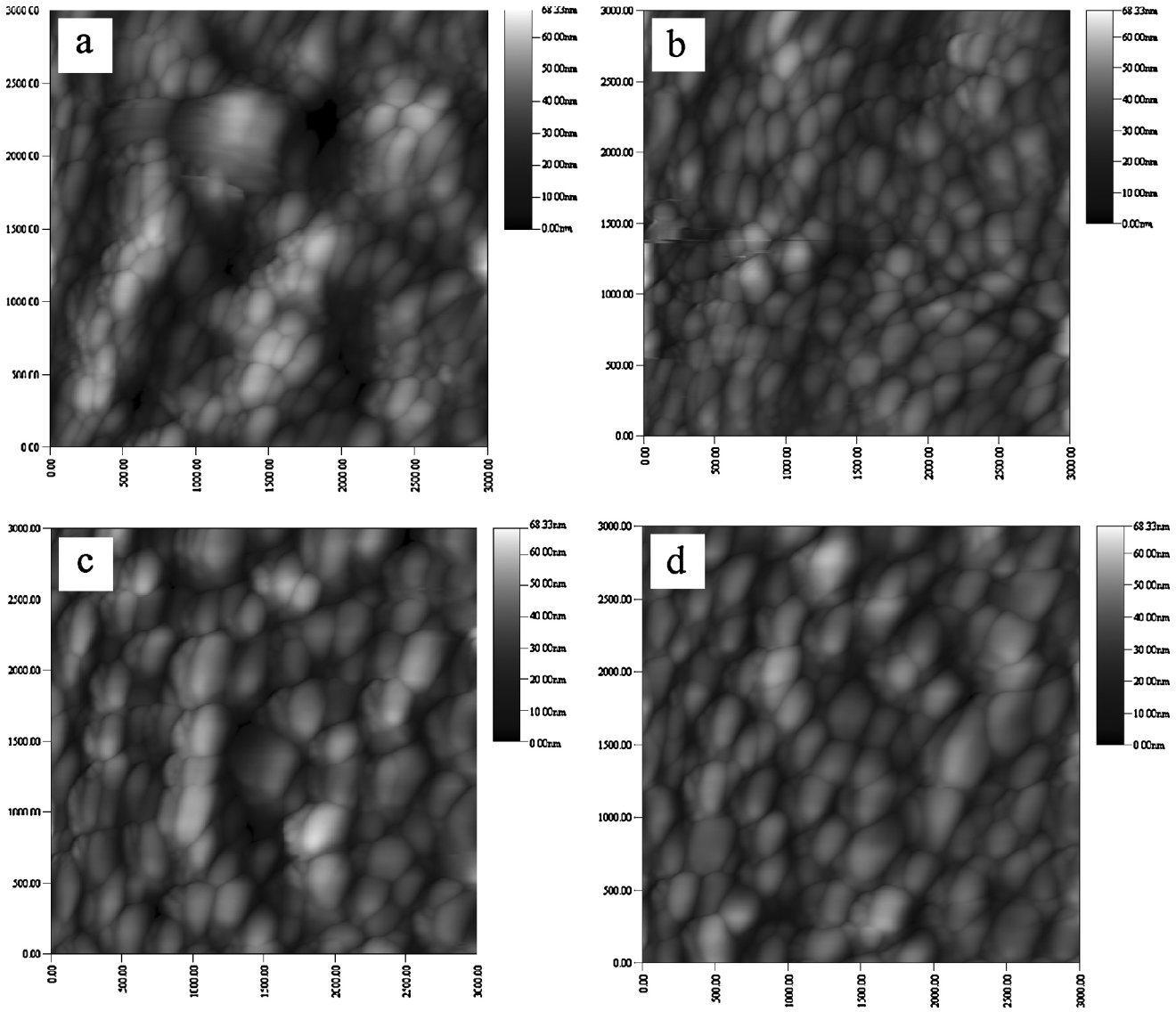

Fig. 4. AFM images of $Mg_xZn_{1-x}O$ thin films annealed at 600 °C: x = 0.00 (a), 0.05 (b), 0.1 (c), 0.15 (d).

geometric projected area, were calculated by means of Imager software. The r values of all thin films were listed in Table 1.

3.2. Optical properties of $Mg_xZn_{1-x}O$ thin films

FTIR spectra of $Mg_{0.15}Zn_{0.85}O$ thin films at different annealing temperature and $Mg_xZn_{1-x}O$ thin films annealed at 600 °C are shown in Figs. 5 and 6, respectively. The peak at about 420 cm^{-1} is assigned to Zn—O stretching vibration. The peak at about 1083 cm^{-1} corresponds to Si—O—Si asymmetric stretching vibration. The wave number and intensity of the peak for $Mg_{0.15}Zn_{0.85}O$ thin films increase with the increase of annealing temperature. The result indicates that SiO_2 composition on the silicon surface increases as annealing temperature increases. The peaks at near 1600 cm^{-1} and 2350 cm^{-1} are attributed to bending vibrations of H—O—H bonds and asymmetrical stretch of C—O which come from moisture and CO_2 on the thin film surface or in the air during the testing process. Low frequency absorption peak of C—H stretching vibration appears at near 2919 cm^{-1}.

Fig. 7 shows room temperature PL spectra of $Mg_{0.15}Zn_{0.85}O$ thin films at different annealing temperature. It can be seen that all the thin films contain a weak ultraviolet emission and a relatively

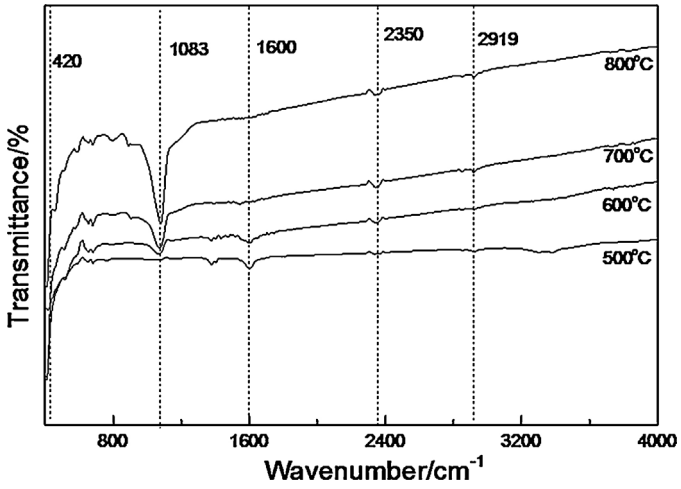

Fig. 5. FTIR spectra of $Mg_{0.15}Zn_{0.85}O$ thin film at different annealing temperature.

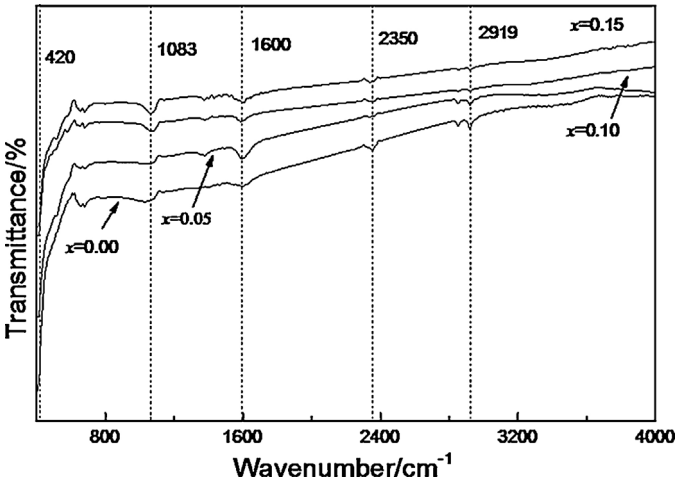

Fig. 6. FTIR spectra of $Mg_xZn_{1-x}O$ thin films annealed at 600 °C.

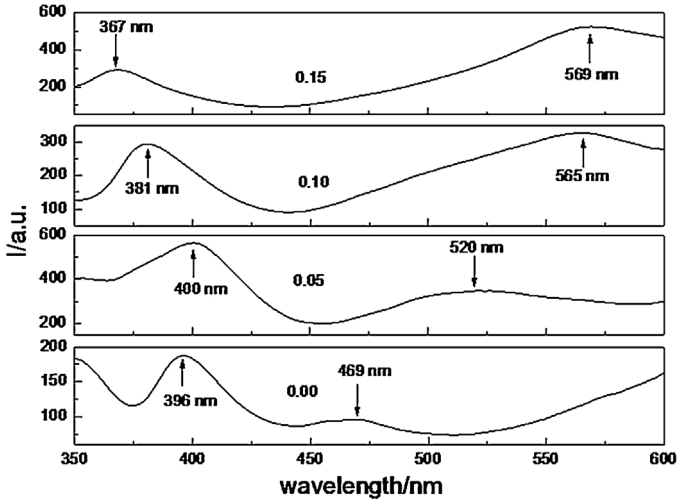

Fig. 8. Room temperature PL spectra of $Mg_xZn_{1-x}O$ thin film annealed at 600 °C.

strong broad visible emission. The ultraviolet emission peak redshifts from 365 nm to 376 nm as annealing temperature increases. The ultraviolet emission is closely related to the electron transition from the conduction band to the valance band [22,23]. The shift of the ultraviolet emission may be attributed to crystallite quality [24,25]. The broad visible emission may be composed of green and yellow emission. Generally, the origin of the green emission may come from oxygen vacancies (V_o) [26] and the yellow emission is associated with interstitial oxygen (O_i) [27]. The intensity of the visible emission increases and its peak position redshifts firstly and then blueshifts as annealing temperature increases. The results indicate that the annealing temperature has an important effect on the number of V_o and O_i in the thin films.

Fig. 8 shows that room temperature PL spectra of $Mg_xZn_{1-x}O$ thin films annealed at 600 °C. The spectra show an ultraviolet emission and a broad visible emission. As the Mg doping changes from 0 to 0.15, the peak position of ultraviolet emission redshifts firstly and then blueshifts. The ultraviolet emission originates from the electron transition between the conduction band and the valance band. The redshift of ultraviolet emission may be related to crystallite quality and Mg doping in the ZnO thin film [28]. The blueshift of ultraviolet emission can be explained by Burstein–Moss effect [29]. It is well know that ZnO is naturally *n*-type material, and the Fermi level will be inside to the conduction band when it is heavily doped. For the higher Mg doped ZnO thin films, the states below Fermi level are occupied by electrons. The electron transition occurs between Fermi level in the conduction band and valance band. Therefore, the blueshift of ultraviolet emission has been observed. In addition, the broad visible emission consists of green and yellow emission. The emission peak intensity enhances gradually and its peak position redshifts to long wavelength from blue to yellow as Mg doping increases from 0 to 0.15. Therefore, Mg doping may change the number of V_o and O_i in the thin films [30].

3.3. Photocatalytic activities of $Mg_xZn_{1-x}O$ thin films

The photocatalytic activities of $Mg_xZn_{1-x}O$ thin films were investigated on degradation of methyl orange (MO). Prior to the photocatalytic degradation of MO in the presence of $Mg_xZn_{1-x}O$ thin films, control experiment for similar experimental conditions but without $Mg_xZn_{1-x}O$ thin films (direct photolysis) has been performed. UV–vis absorption spectra of methyl orange after different irradiation times using $Mg_{0.15}Zn_{0.85}O$ thin films annealed at 600 °C as photocatalyst are shown in Fig. 9. The absorbance peak of methyl orange using $Mg_{0.15}Zn_{0.85}O$ thin films annealed at 600 °C is at 464 nm and the intensities decrease with the increase of the irradiation time, and the concentration of methyl orange reduced

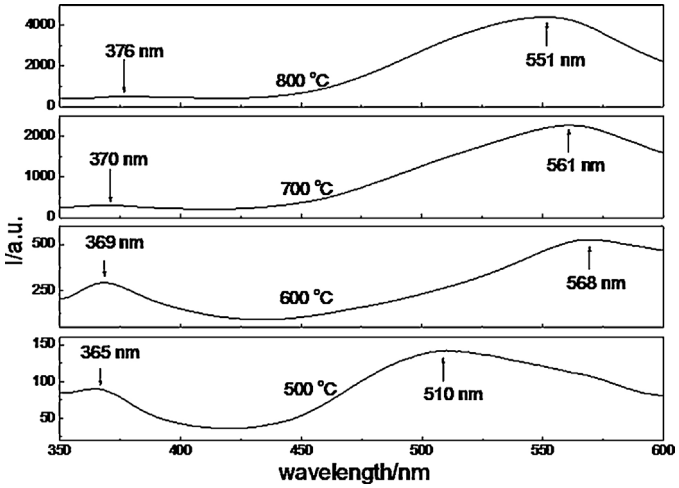

Fig. 7. Room temperature PL spectra of $Mg_{0.15}$ $Zn_{0.85}$ O thin film at different annealing temperature.

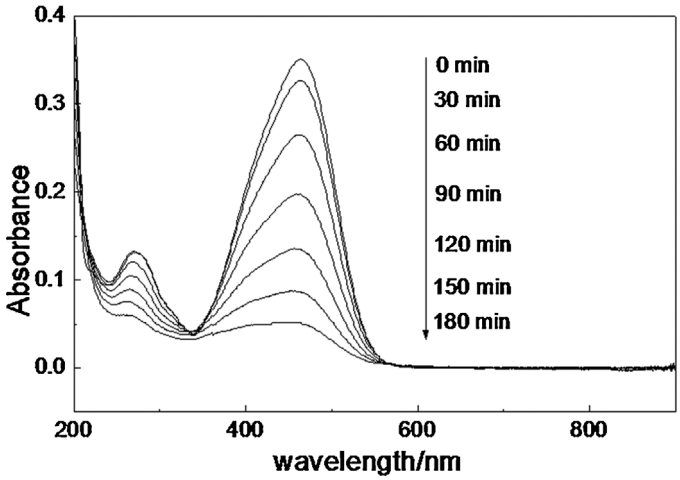

Fig. 9. UV–vis absorption spectra of MO after different irradiation times using $Mg_{0.05}Zn_{0.95}O$ thin film annealed at 600 °C as photocatalysts.

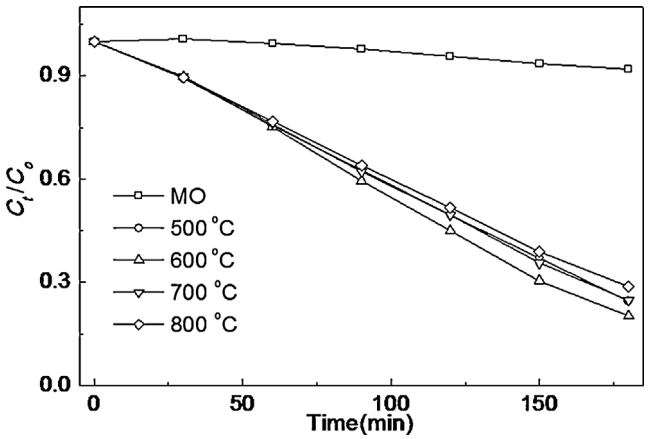

Fig. 10. Photodegradation curves of MO using $Mg_{0.15}Zn_{0.85}O$ thin film annealed at different annealing temperature as photocatalysts.

as much as 85.8% after 180 min. The photocatalytic degradation of methyl orange is believed to perform according to the following mechanisms. Electrons in the valence band are excited to the conduction band and leave holes in the valence when the $Mg_xZn_{1-x}O$ thin films absorbs a UV photon with energy equal to or greater than its band gap.

$$ZnO + h\nu \rightarrow ZnO(e^- + h^+) \quad (3)$$

$$h^+ + H_2O \rightarrow OH^* + H^+ \quad (4)$$

$$e^- + O_2 \rightarrow O_2^- \quad (5)$$

$$O_2^- + H^+ \rightarrow HO_2^* \quad (6)$$

$$HO_2^* + O_2^- + H^+ \rightarrow H_2O_2 + O_2 \quad (7)$$

$$H_2O_2 + e^- \rightarrow OH^- + OH^* \quad (8)$$

$$OH^* + \text{dye} \rightarrow \text{degraded dye} \quad (9)$$

The absorbance of the solution at 464 nm was chosen as the measurement of the MO concentration. The ratios of the absorbance of MO solution after irradiation for t min to that of MO solution before irradiation correspond to relative concentration C_t/C_0. Fig. 10 shows the curves of C_t/C_0 versus irradiation time for the $Mg_{0.15}Zn_{0.85}O$ thin films and without thin film. It can be seen that self-photolysis of methyl orange under UV irradiation is so little and can be neglected. Fig. 11 shows the curves of C_t/C_0 versus irradiation time for the

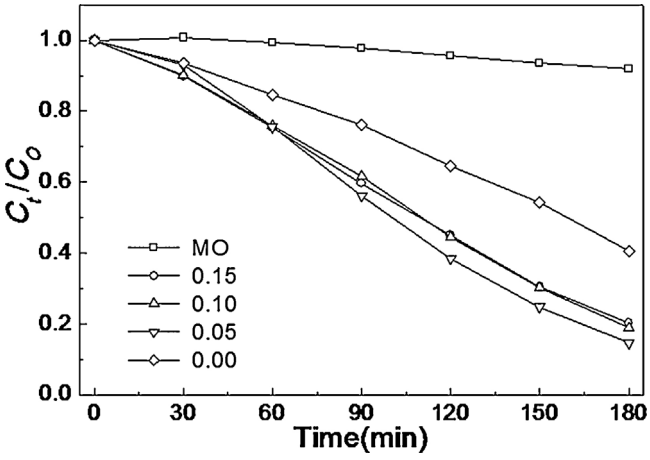

Fig. 11. Photodegradation curves of MO using $Mg_xZn_{1-x}O$ thin film annealed at 600 °C as photocatalysts.

$Mg_xZn_{1-x}O$ thin films annealed at 600 °C. The photocatalytic degradation efficiency of the samples after 180 min UV irradiation were listed in Table 1. Jongnavakit et al. [31] thought that the enhanced photocatalytic activity may be caused by the improving of the crystallinity and the surface roughness of ZnO thin films with the increase of annealing temperature. Wang et al. [32] reported that the ZnO nanocrystals with a high concentration of oxygen defects exhibit excellent photocatalytic activity. The oxygen defects are proposed to be the active sites of the ZnO photocatalyst. Kenanakis et al. [33] studied the photocatalytic properties of ZnO thin films and nanostructures. All samples exhibit remarkable photocatalytic activity, which may be due to their good crystallinity and large surface area. Zhang et al. [34] suggested the enhanced photocatalytic activity of the hexagonal faceted ZnO quantum dots may be attributed to the large specific surface areas, special hexagonal morphology and surface oxygen vacancies. Suwanboon et al. [35] thought that the decrease of photocatalytic degradation for $Zn_{0.90}Mg_{0.10}O$ might be due to the formation of an amorphous MgO on the surface of catalyst.

In this paper, it was noticeable that pure ZnO thin film annealed at 600 °C has the lowest photocatalytic degradation efficiency. The increase of photocatalytic degradation efficiency of all the $Mg_xZn_{1-x}O$ thin film may be attributed to the increase of grain size, roughness factor and oxygen defects. For all the thin films, the $Mg_{0.05}Zn_{0.95}O$ thin films annealed at 600 °C exhibits the highest photocatalytic degradation efficiency, and the concentration of methyl orange reduced as much as 85.8%. It also can be seen that the photocatalytic degradation efficiency of the $Mg_xZn_{1-x}O$ thin film annealed at 600 °C increases firstly and then decreases as x value increases from 0 to 0.15. The photocatalytic degradation efficiency of $Mg_{0.15}Zn_{0.85}O$ thin film increases to a maximum when the annealing temperature increases to 600 °C, and then decreases with increasing annealing temperature. The results may be attributed to the increase of amorphous MgO on the surface of thin film as Mg concentration or annealing temperature increase. Therefore, changes of the photocatalytic activities of the thin films are a synergistic effect defined by grain size, roughness factor, oxygen defects and amorphous MgO.

4. Conclusions

In conclusion, $Mg_xZn_{1-x}O$ thin films were successfully synthesized on Si substrates by sol–gel method. The XRD and AFM results reveal that the mean grain size, preferential orientation and surface roughness of $Mg_xZn_{1-x}O$ thin films were affected by the annealing temperature and Mg doping concentration. The FTIR spectra show that the peak at about 420 cm^{-1} is assigned to Zn—O stretching vibration. The peak at 1083 cm^{-1} belongs to Si—O—Si asymmetric stretching vibration. The PL spectra of the samples were mainly composed of an ultraviolet emission and a broad visible emission. The green emission can be ascribed to oxygen vacancy (V_o) and the yellow emission may come from oxygen interstitial (O_i). The results of the photocatalytic degradation of MO show that the annealing temperature and Mg doping concentration have an effect on photocatalytic activity of $Mg_xZn_{1-x}O$ thin films. The $Mg_{0.05}Zn_{0.95}O$ thin film annealed at 600 °C exhibits the highest photocatalytic degradation efficiency. The variety of photocatalytic activity of $Mg_xZn_{1-x}O$ thin films may be ascribed to the change of grain size, roughness factor, oxygen defects and amorphous MgO.

Acknowledgements

This work was supported by State Key Program for Basic Research of China (2013CB632705), National Natural Science Foundation of China (Nos. 11334008, 61290301, 51072001, 51272001,

51002156, 51102072), China Postdoctoral Science Foundation (No. 2012M520944), Anhui Provincial Natural Science Foundation (No. 1208085MF99, 1208085QA16), Natural Science Foundation of Anhui Higher Education Institution of China (No. KJ2012Z336), Shanghai Postdoctoral Science Foundation (No. 12R21416800), Funds for Distinguished Young Scholar of Anhui University (No. KJJQ1103).

References

[1] Y. Natsume, H. Sakata, Thin Solid Films 372 (2000) 30–36.
[2] G.K. Paul, S. Bandyopadhyay, S.K. Sen, Phys. Status Solidi A 191 (2002) 509–518.
[3] M.W. Ahn, K.S. Park, J.H. Heo, D.W. Kim, K.J. Choi, J.G. Park, Sens. Actuators B: Chem. 138 (2009) 168–173.
[4] J. Yi, J.M. Lee, W.I. Park, Sens. Actuators B: Chem. 155 (2011) 264–269.
[5] C.R. Gorla, N.W. Emanetoglu, S. Liang, W.E. Mayo, Y. Lu, M. Wraback, H. Shen, J. Appl. Phys. 85 (1999) 2595–2602.
[6] Y. Chen, N.T. Tuan, Y. Segawa, H.J. Ko, S.K. Hong, T. Yao, Appl. Phys. Lett. 78 (2001) 1469–1471.
[7] J.C.S. Wu, C.H. Chen, J. Photochem. Photobiol. A: Chem. 163 (2004) 509–515.
[8] A. Ohtomo, M. Kawasaki, T. Koida, K. Masubuchi, H. Koinuma, Y. Sakurai, Y. Yoshida, T. Yasuda, Y. Segawa, Appl. Phys. Lett. 72 (1998) 2466–2468.
[9] X. Qiu, Y. Xue, G. Li, L. Li, Chem. Lett. 36 (2007) 384–385.
[10] N.B. Chen, C.H. Sui, Mater. Sci. Eng. B 126 (2006) 16–21.
[11] C.A.K. Gouvea, F. Wypych, S.G. Moraes, N. Duran, N. Nagata, P. Peralta-Zamora, Chemosphere 40 (2000) 433–440.
[12] B. Dindar, S. Icli, J. Photochem. Photobiol. A: Chem. 140 (2001) 263–268.
[13] M.C. Yeber, J. Rodriguez, J. Freer, N. Duran, H.D. Mansilla, Chemosphere 41 (2000) 1193–1197.
[14] Q. Wan, T.H. Wang, J.C. Zhao, Appl. Phys. Lett. 87 (2005), 083105–083105-3.
[15] Y. Tong, J. Cheng, Y. Liu, G.G. Siu, Scripta Mater. 60 (2009) 1093–1096.
[16] M. Dutta, D. Basak, Nanotechnology 20 (2009) 475602.
[17] F. Meng, X. Song, Z. Sun, Vacuum 83 (2009) 1147–1151.
[18] J.J. Ding, H.X. Chen, S.Y. Ma, Appl. Surf. Sci. 256 (2010) 4304–4309.
[19] S. Kumar, V. Gupte, K. Sreenivas, J. Phys.: Condens. Matter 18 (2006) 3343.
[20] J. Lv, C. Liu, W. Gong, Z. Zi, X. Chen, K. Huang, T. Wang, G. He, X. Song, Z. Sun, Superlattices Microstruct. 51 (2012) 886–892.
[21] C. Sun, L.Q. Ge, Z.Z. Gu, Thin Solid Films 515 (2007) 4686–4690.
[22] R. Ajimsha, R. Manoj, P. Aneesh, M. Jayaraj, Curr. Appl. Phys. 10 (2010) 693–697.
[23] B. Lin, F. Zhuxi, Y. Jia, Appl. Phys. Lett. 79 (2001) 943–945.
[24] D. Behera, B.S. Acharya, J. Lumin. 128 (2008) 1577–1586.
[25] S. Cho, J. Ma, Y. Kim, Y. Sun, G.K.L. Wong, J.B. Ketterson, Appl. Phys. Lett. 75 (1999) 2761–2763.
[26] K. Vanheusden, W.L. Warren, C.H. Seager, D.R. Tallant, J.A. Voigt, B.E. Gnade, J. Appl. Phys. 79 (1996) 7983–7990.
[27] X.L. Wu, G.G. Siu, C.L. Fu, H.C. Ong, Appl. Phys. Lett. 78 (2001) 2285–2287.
[28] Ü. Özgür, I. Alivov Ya, C. Liu, A. Teke, M.A. Reshchikov, S. Doğan, V. Avrutin, S.J. Cho, H. Morkoç, J. Appl. Phys. 98 (2005) 041301.
[29] J. Yang, X. Zhao, X. Shan, H. Fan, L. Yang, Y. Zhang, X. Li, J. Alloy. Compd. 556 (2013) 1–5.
[30] X. Liu, X. Wu, H. Cao, R.P.H. Chang, J. Appl. Phys. 95 (2004) 3141–3147.
[31] P. Jongnavakit, P. Amornpitoksuk, S. Suwanboon, T. Ratana, Thin Solid Films 520 (2012) 5561–5567.
[32] J. Wang, P. Liu, X. Fu, Z. Li, W. Han, X. Wang, Langmuir: ACS Surf. Colloids 25 (2009) 1218–1223.
[33] G. Kenanakis, Z. Giannakoudakis, D. Vernardou, C. Savvakis, N. Katsarakis, Catal. Today 151 (2010) 34–38.
[34] L. Zhang, L. Yin, C. Wang, N. Lun, Y. Qi, ACS Appl. Mater. Interfaces 2 (2010) 1769–1773.
[35] S. Suwanboon, P. Amornpitoksuk, P. Bangrak, N. Muensit, Ceram. Int. 39 (2013) 5597–5608.